NASA Technical Memorandum 4646

Determination of Stores Pointing Error Due to Wing Flexibility Under Flight Load

William A. Lokos, Catherine M. Bahm, and Robert A. Heinle

January 1995

NASA Technical Memorandum 4646

Determination of Stores Pointing Error Due to Wing Flexibility Under Flight Load

William A. Lokos, Catherine M. Bahm,
and Robert A. Heinle
Dryden Flight Research Center
Edwards, California

National Aeronautics and
Space Administration
Office of Management
Scientific and Technical
Information Program
1995

ABSTRACT

The in-flight elastic wing twist of a fighter-type aircraft was studied to provide for an improved on-board real-time computed prediction of pointing variations of three wing store stations. This is an important capability to correct sensor pod alignment variation or to establish initial conditions of iron bombs or smart weapons prior to release. The original algorithm was based upon coarse measurements. The electro-optical Flight Deflection Measurement System measured the deformed wing shape in flight under maneuver loads to provide a higher resolution database from which an improved twist prediction algorithm could be developed. The FDMS produced excellent repeatable data. In addition, a NASTRAN finite-element analysis was performed to provide additional elastic deformation data. The FDMS data combined with the NASTRAN analysis indicated that an improved prediction algorithm could be derived by using a different set of aircraft parameters, namely normal acceleration, stores configuration, Mach number, and gross weight.

NOMENCLATURE

AMRAAM	advanced medium range air-to-air missile
CG	center of gravity
FDMS	Flight Deflection Measurement System
FEA	finite-element analysis
h	pressure altitude, ft
IMU	inertial measurement unit
INU	inertial navigation unit
LED	light emitting diode
M	Mach number
NASTRAN	NASA structural analysis program
Nz	normal acceleration, g
NzW	product of normal acceleration and aircraft gross weight
PCM	pulse code modulation

INTRODUCTION

This investigation studied the in-flight spanwise elastic wing twist distribution of an F-16C Block 40 aircraft to determine pointing error of three wing store stations during maneuvering flight. The evolution of various precision airborne remote sensors has led to interest in quantifying aircraft elastic deformations in flight. When a directional sensor is mounted on one part of an aircraft and its point of reference is another part of the aircraft, the elastic deformation of the structure between the two points produces a variable alignment error that cannot simply be zeroed out. Wing-mounted devices are particularly vulnerable to variable misalignment caused by structural elasticity. Determining the elastic wing twist distribution is also valuable for establishing the initial conditions of iron bombs or smart weapons prior to release.

A previous attempt to quantify the in-flight deformation of the F-16 wing involved the use of dummy store objects which were each instrumented with an attitude sensing gyroscopic device called an Inertial Measurement Unit (IMU). Although there were some problems with the resulting flight data repeatability and accuracy, this effort culminated in an algorithm which can predict wing store pitch, roll, and yaw variation in a real-time mode using an existing onboard computer.

To obtain higher quality, repeatable wing deformation data, an F-16 aircraft was instrumented with the electro-optical Flight Deflection Measurement System (FDMS) and a flight test program was performed. Because it was not possible to fully flight test all useful combinations of Mach, altitude, normal acceleration, gross weight, stores loading, etc., a NASTRAN finite-element analysis (FEA) was also performed. The additional data provided by this analysis allowed broader investigation of parametric influences on wing twist, especially concerning aircraft gross weight effect.

This paper describes the study of the F-16 spanwise elastic wing twist distribution. Algorithm and FEA predictions are compared with FDMS flight-measured data. Subject flight conditions are for 0.9 and 1.2 M, 5,000- and 20,000-ft altitude, 1- to 5-g normal acceleration, and for a variety of aircraft gross weights and stores loadings. All store configurations studied were symmetrical. These flight conditions were selected based on availability of flight data and aircraft operational considerations. Recommendations are given for parameter selection for an improved wing twist prediction algorithm. This investigation involved quasi-steady-state symmetrical flight conditions and therefore does not account for the effects of roll acceleration or roll rate, which could be significant in an antisymmetric maneuver.

AIRCRAFT DESCRIPTION

The test aircraft, an F-16C Block 40, is a light weight, single seat, double-sonic jet fighter. It is capable of up to 9-g maneuvering flight. It is fitted with provisions for up to nine store stations including four on each wing and one under the fuselage centerline. Figure 1 illustrates the store station locations. These stations can carry an assortment of hardware including fuel tanks, electronic counter-measure pods, sensor pods, iron bombs, precision guided bombs, air-to-ground missiles, air-to-air missiles, and other devices. The wing is all metallic with aluminum alloy skins and substructure. It has a low aspect ratio and uses multiple spars. The wing box structure is sealed and carries fuel. A leading-edge flap and flaperon are fitted. The F-16 is well known around the world and further information is available from a variety of sources.[1]

FLIGHT DEFLECTION MEASUREMENT SYSTEM DESCRIPTION

FDMS Hardware

The electro-optical FDMS was originally developed by Grumman for NASA use on the Highly Maneuverable Aircraft Technology (HiMAT) remotely piloted research vehicle.[2] This FDMS design was modified to extend the system operating range (maximum allowable distance from receiver to target) for use on the X-29A forward-swept-wing aircraft[3] because of its larger wing span. The range was again increased, through circuit modification, for use by NASA with the Advanced Fighter Technology Integration (AFTI) F-111 Mission Adaptive Wing research aircraft.[4] This third FDMS hardware version was the type employed on the F-16. Figure 2 is a photo of this hardware and a system operation diagram. The FDMS consists of a control unit, a target driver, 2 receivers, and 16 infrared light emitting diode (LED)

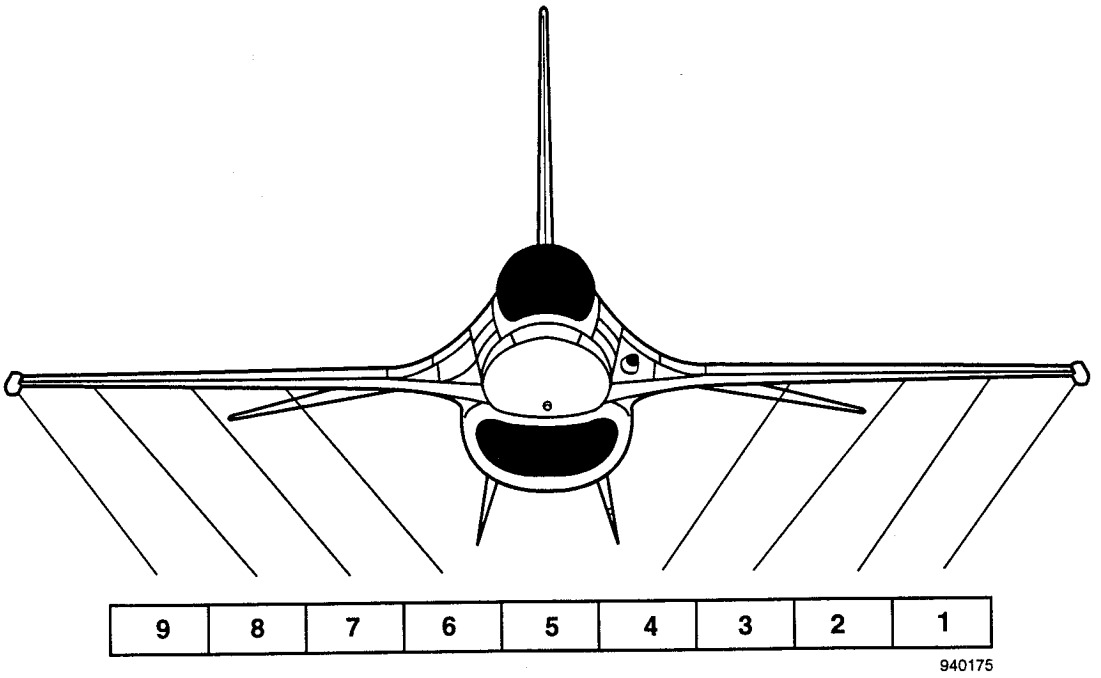

Fig. 1 F-16 external store stations.

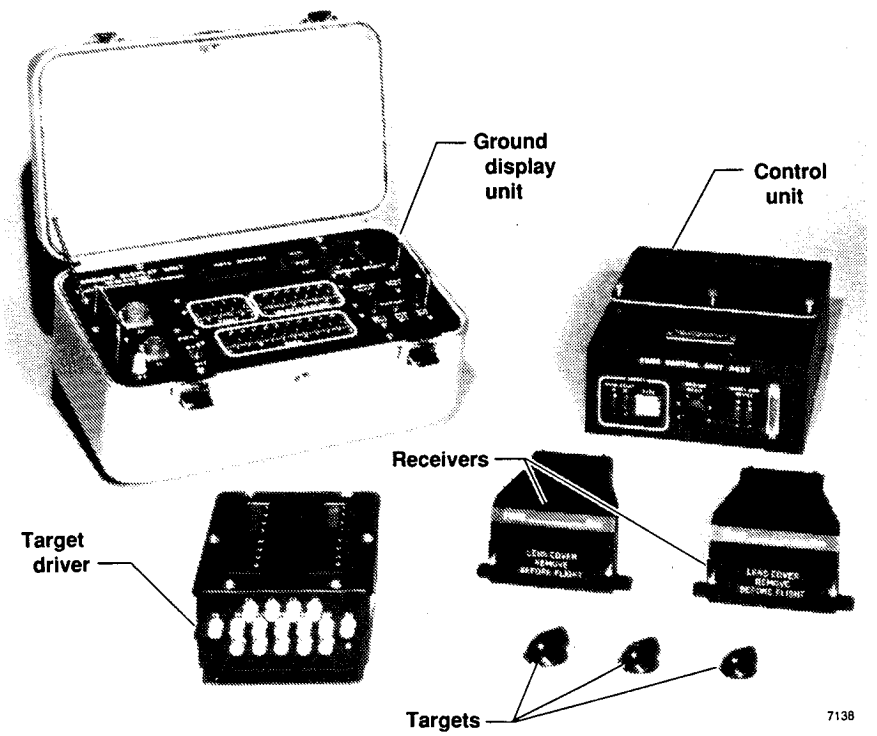

(a) Hardware.

Fig. 2 FDMS hardware and system diagram.

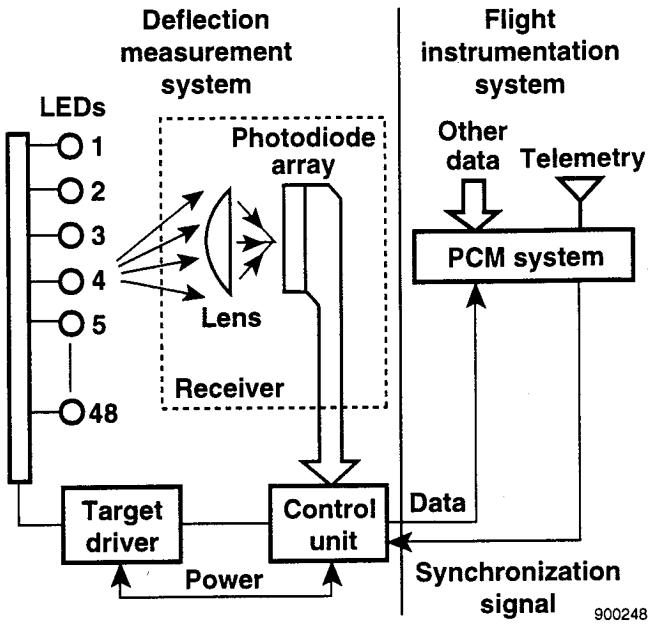

(b) System diagram.

Fig. 2 Concluded.

targets. Hardware provisions exist for up to 48 targets and up to 6 receivers although they were not needed for this application. The targets each consist of an LED, a reflector, and an aluminum housing. The receiver design uses a 512-element linear, photo-sensitive, charge-coupled diode array as the actual sensing device.

Each light image input to the receiver is focused as a horizontal line that is perpendicular to the array axis. The location of the focused line on the diode array determines the displacement value for that sample. The target driver is used to energize the LEDs sequentially. Each driver can actuate up to 16 targets. The control unit coordinates the operation of the target driver(s) and receivers and also interfaces with the aircraft pulse code modulation (PCM) data system. The control unit uses the PCM end-of-frame pulse as a synchronization signal. This signal must be available approximately every 5 msec. After each synchronization signal, the appropriate receiver's array is initialized and then, with no target illuminated, the background light is sampled. While the target driver illuminates an LED, the array is scanned again. After signal processing, the control unit then outputs two 10-bit digital words to the PCM system. One word contains the target identification and error information concerning the receiver signal. The other word contains the position of that target on the diode array. With the next synchronization signal, the location of the next target is sampled and reported to the PCM system. In this manner all targets are sampled, one every 5 msec. With a typical 16-target installation, each target will be sampled every 80 msec or 12 1/2 times/sec. This sampling rate is adequate for quasi-static structural measurements, even for high-rate maneuvers such as abrupt pull-ups. Reference 5 further describes the operational aspects of this FDMS.

F-16 FDMS Installation

The target layout used with the F-16 is shown in Figure 3. The targets were located on the upper surface of the right-hand wing, at five span stations, primarily along the front spar, rear spar, and an

intermediate line between the two. As only symmetrical flight cases were studied, only one side of the aircraft was instrumented. The photo in Figure 4 shows the targets partially installed. The view is looking inboard and aft from the right-hand wingtip. The wingtip missile launch rail (not shown) was equipped with four targets. All targets were aligned in two axes so that they would project their light output on the receiver window, at ground rest and throughout the expected flight deflection range. This alignment was facilitated through the use of wedge shaped micarta spacers installed between the target housings and the surface of the wing. These spacers also provided electrical insulation of the target housings from the wing skin. The target driver's wires were routed internally along the front spar, penetrated a cover panel at four locations and then ran generally chordwise along the surface to each target. This surface wiring was bonded to the wing using gray polysulfide fuel tank sealant. This same compound was used to attach the targets to the wing skin. The flexible bond produced has proven to be tough and trouble free under all flight test conditions encountered to date. Also visible in Figure 4 is the receiver bay at the root of the vertical tail. In this photo the window panel is removed, revealing the receivers and associated mounting structure. Figure 5 is a close-up photo of this area. Two independently adjustable receiver mounts are supported by a common shelf structure which, in turn, is attached to substantial aircraft structure. The mounting structure and the manner of attachment to the aircraft were designed to maximize stiffness to preclude erroneous deflection sensing caused by local flexibility of the receiver mount. This was verified during initial calibration by manually applying vertical load to the receivers while simultaneously monitoring the system output and observing no change. The front receiver has a 10-cm focal length and views the 6 most inboard targets. The aft receiver has a 20-cm focal length and views the outboard 10 targets. This combination of two receivers of different focal lengths was chosen to fulfill the requirement for field-of-view coverage and optimum resolution.

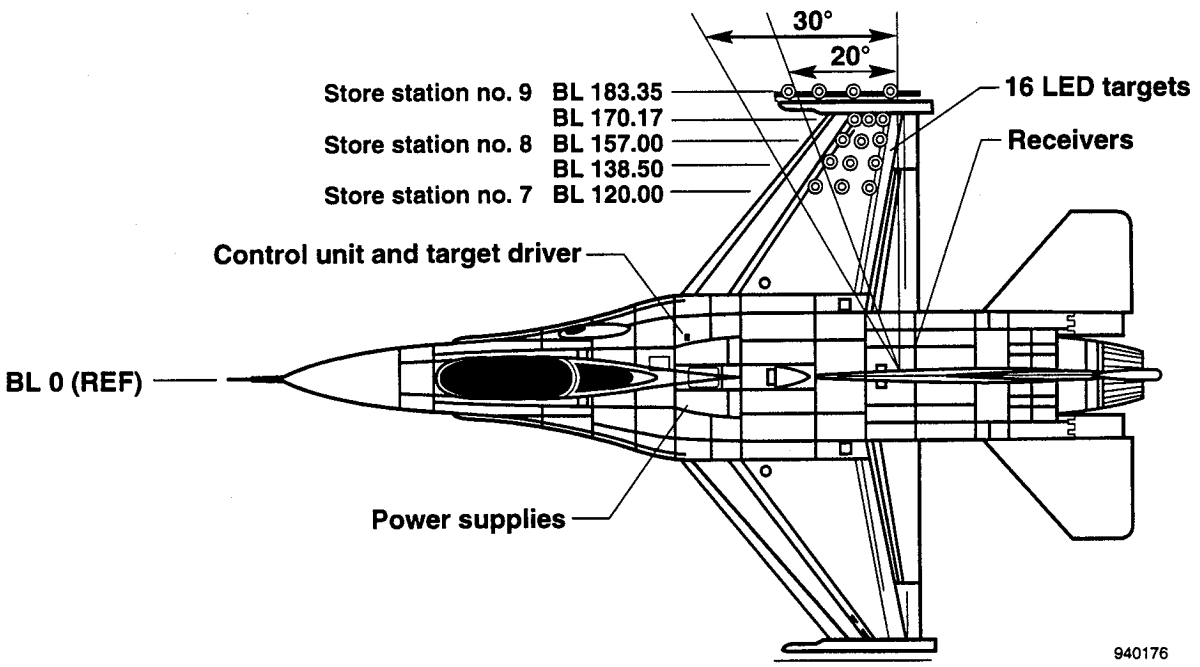

Fig. 3 FDMS installation.

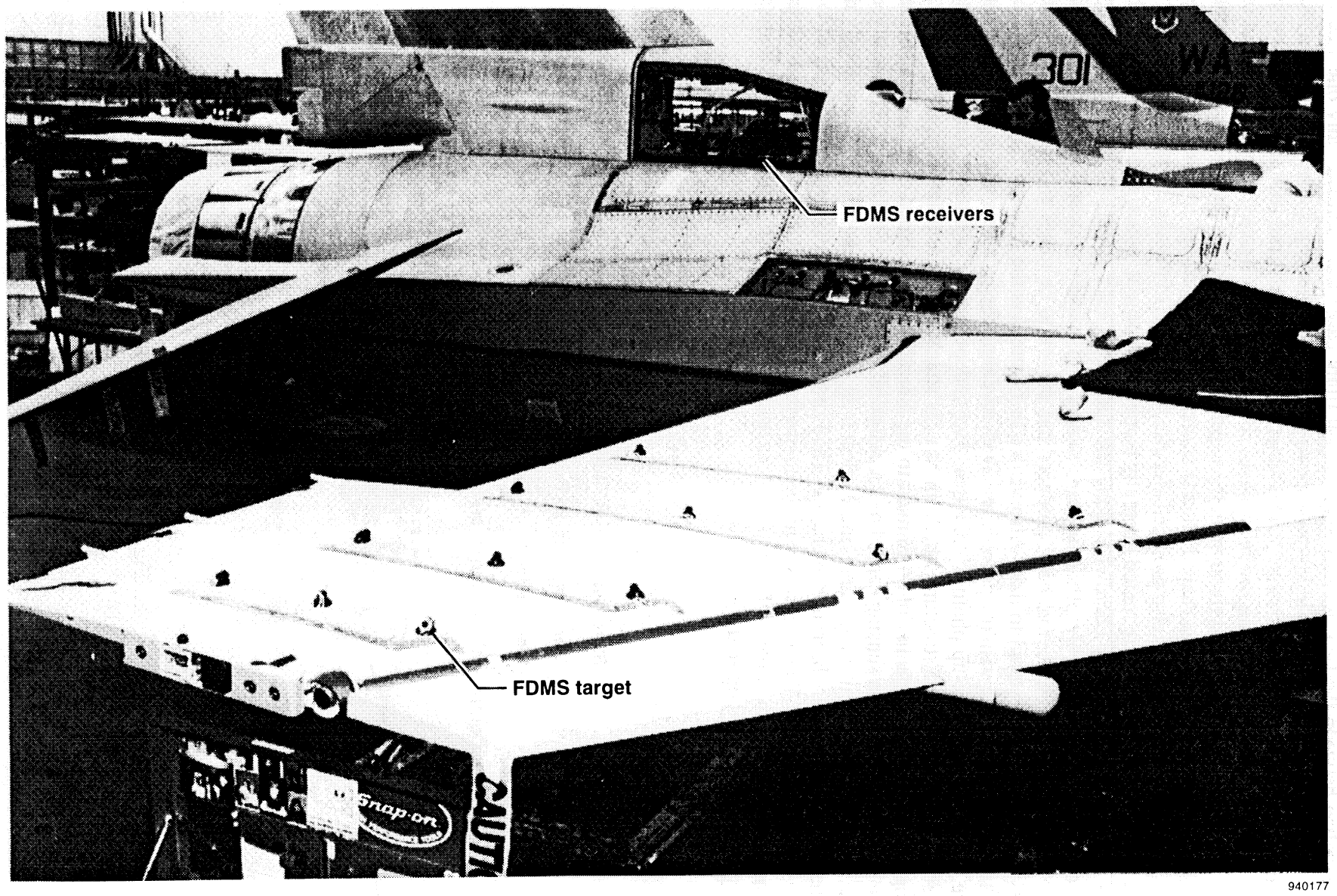

Fig. 4 F-16 showing partially installed FDMS targets and receivers.

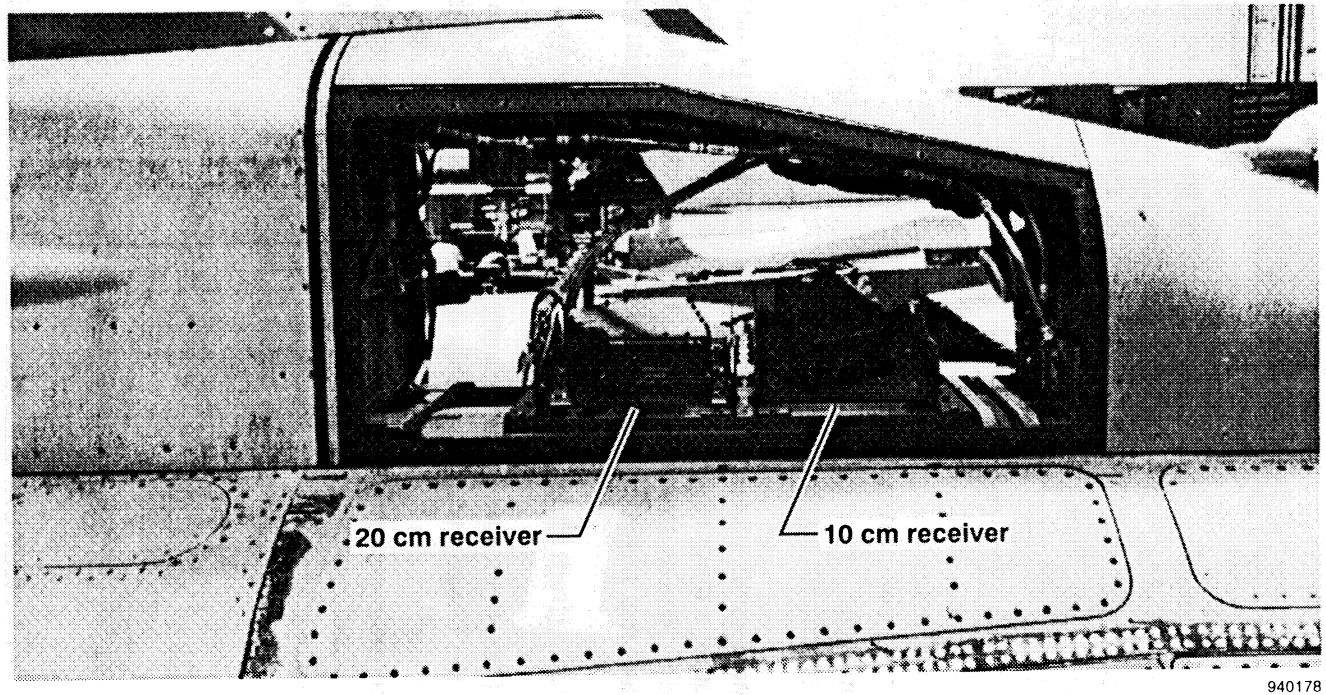

Fig. 5 Receiver bay.

Figure 6 is a photo of the right-hand wing from just above the receiver bay. This view shows all 16 targets installed. This photo is unusual in that it was taken with infrared sensitive film. The FDMS was operating as the photo was taken. Each target is shown producing a light signal. All targets appear illuminated at once because the exposure time was greater than the 80 msec required to cycle though all targets once. The purpose of the infrared photo was to search for possible target reflection problems. None were found due mainly to the matte gray finish of this aircraft.

FDMS ACCURACY

An important consideration with any measurement device or system is the accuracy of its measurements. Figure 7 gives deflection and twist resolution magnitudes for each span station instrumented. The deflection resolution is dependent upon the receiver focal length and the distance of the target from the receiver. The twist resolution is dependent upon the deflection resolution and the chord spacing between the front and rear targets used to calculate the twist at that span station. The FDMS resolved the vertical field of view of each receiver into 1024 data counts. The 10-cm focal length receiver had a vertical field of view of 14° while the 20-cm focal length receiver had a vertical field of view of 7°. The broadest possible error band of a single measurement is ± 2 counts. Added to this is the calibration error, which can be reduced to approximately ± 0.25 count over the range the calibration was performed. The effect of calibration error on total measurement system accuracy is negligible. Each target was calibrated over the full range of deflection it could potentially experience in flight.

Because two different focal length receivers were used and targets were positioned at varying distances from the receiver lens planes, a range of values was needed to characterize the deflection measurement precision as installed on the F-16. The streamwise wing box twist was calculated for each instrumented span station from the front and rear target deflections using the following equation:

$$\text{TWIST} = \sin^{-1}[(\text{front target deflection} - \text{rear target deflection})/\Delta \text{ chord}]$$

By using two different focal length receivers and the corresponding pairing of the targets to the receivers, the deflection resolution at the wingtip was noticeably better than that of the inboard station. The twist resolutions shown here are based on the broadest possible error band associated with each target deflection sample, in the worst possible combination. Average deflection and twist errors would be approximately half of these values. If multiple samples are available and data averaging or sloping techniques are used, the resultant error band is even smaller. The typical estimated error in twist measurement for the FDMS flight data in this paper is one third that shown in Figure 7.

PREDICTION TECHNIQUES

Real-Time Algorithm

The current F-16 wing twist prediction algorithm was derived from a previous flight test program which used two identical dummy store objects. Each object contained an attitude sensing device called an inertial measurement unit (IMU). These IMUs were mounted symmetrically under each wing. One span station at a time was studied. Various loadings and flight conditions were flown and the relative differences between the attitudes of the F-16 INU and the two IMUs were compared to determine the store's relative roll, pitch, and yaw. The relative pitch was the largest and most significant variation found and

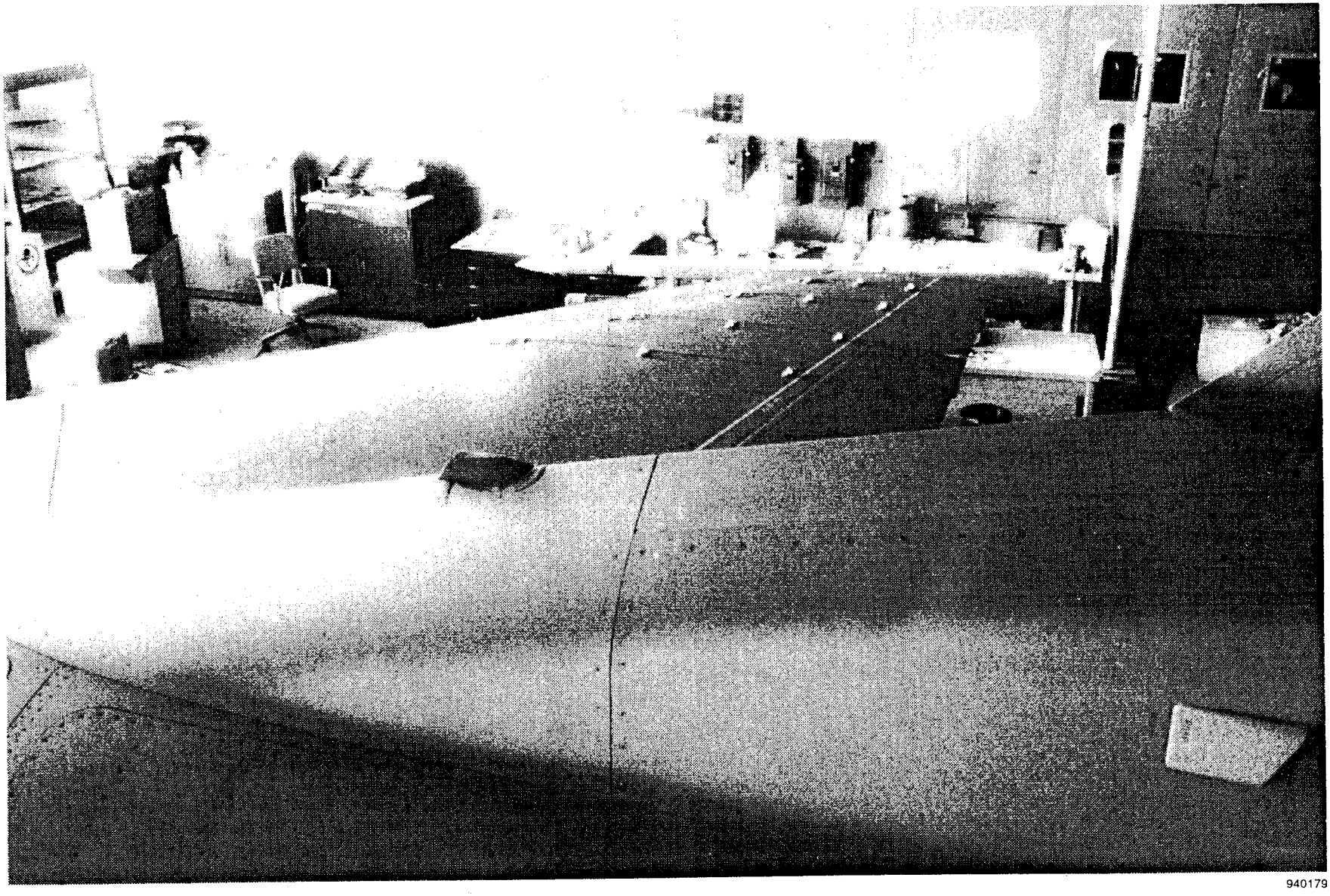

Fig. 6 Right-hand wing.

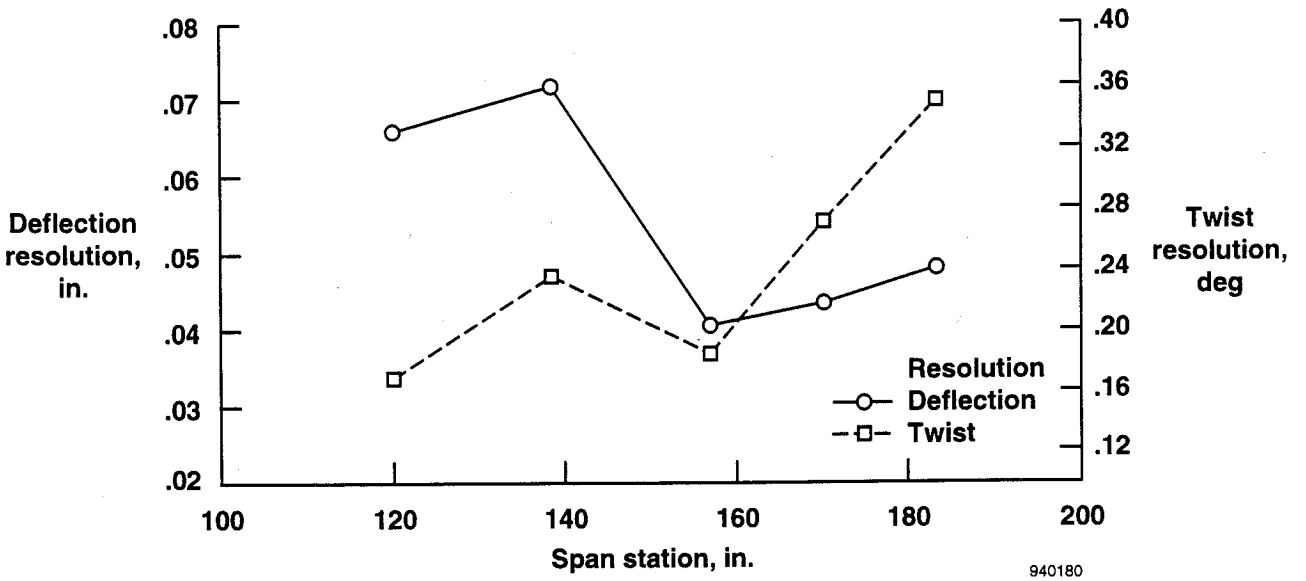

Fig. 7 F-16 FDMS deflection and twist resolution.

this yielded the elastic wing twist for that span station. Unfortunately, comparisons of left- and right-side data sometimes indicated asymmetric twist for symmetrical maneuvers and repeatability was not as good as desired. The IMU-produced data were processed to determine the equation of a best curve fit as a function of aircraft span station, Mach, altitude, and normal acceleration. The resultant pitch, or twist, equation was quite complex, having no less than 13 coefficients.

Finite Element Analysis

A NASTRAN model of the F-16 Block 40 aircraft was obtained from the Lockheed Fort Worth Company. This "coarse-grid" model represents only the right-hand half of the aircraft and has approximately 160,000 degrees of freedom. The model was provided in the form of 17 subcomponent files which were assembled to produce the overall model. The wing model is shown in Figure 8. In addition to the model, 12 predicted load cases were obtained. These distributed net structural load cases represent 1-*g* cruise and 5-*g* symmetrical pull-ups at 5,000- and 20,000-ft altitude at 0.9 *M* and 1.2 *M* with a variety of external stores loading configurations. These cases were selected to compliment the available flight data conditions. To accommodate these varied flight conditions, the model was obtained with two different wing leading-edge flap configurations. These flap configurations were used as needed to replicate the flap positions seen in flight.

RESULTS AND DISCUSSION

Algorithm Predictions

Figure 9 shows algorithm predictions for wing elastic twist versus span for 6 different flight conditions at 5*g*s from 0.6 *M* to 1.2 *M*, at altitudes of 5,000 and 20,000 ft. Positive twist is defined here as trailing edge down. There are two clear trends apparent in this plot. First, for both altitudes, twist is predicted

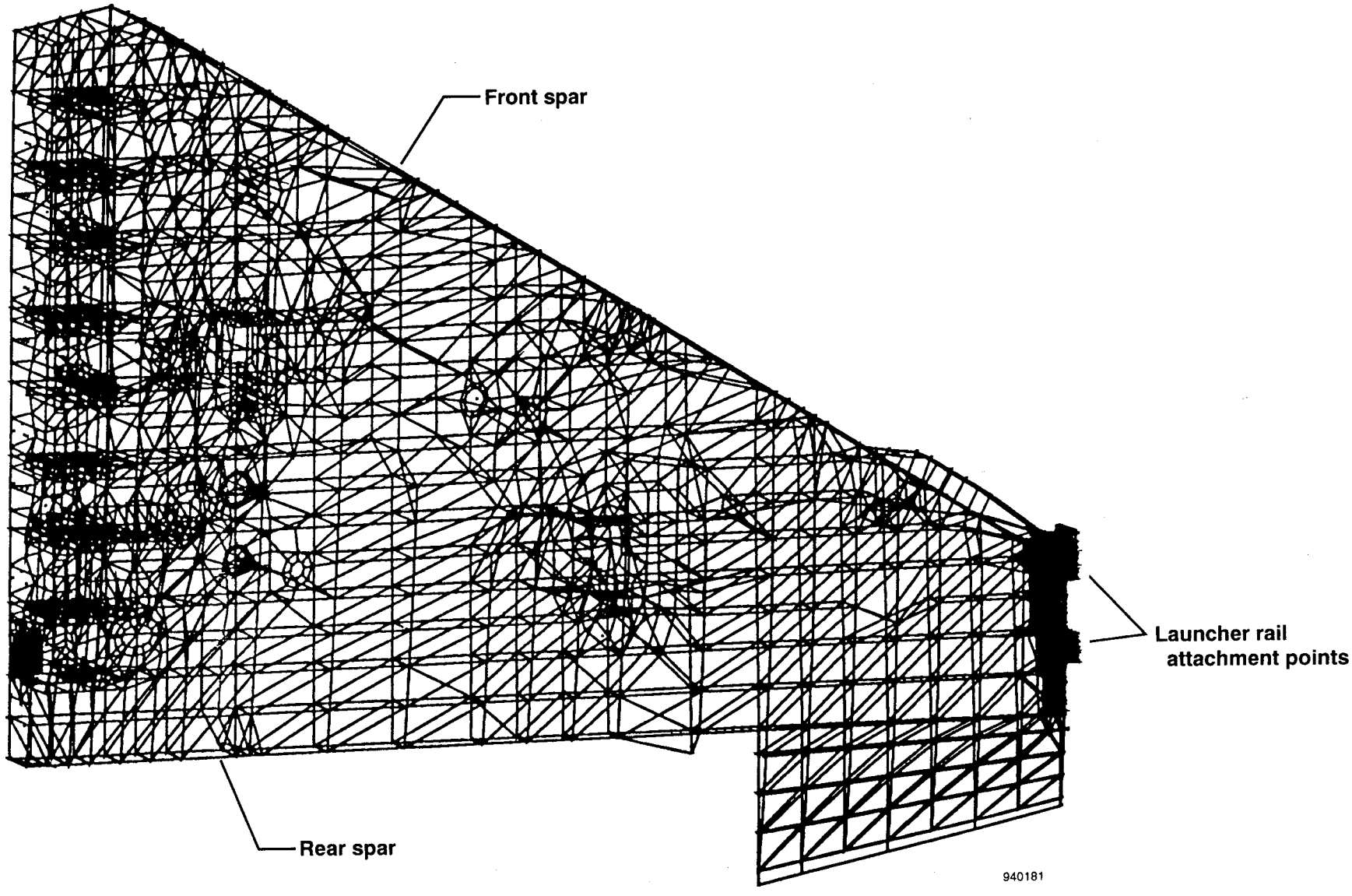

Fig. 8 NASTRAN model of F-16 wing.

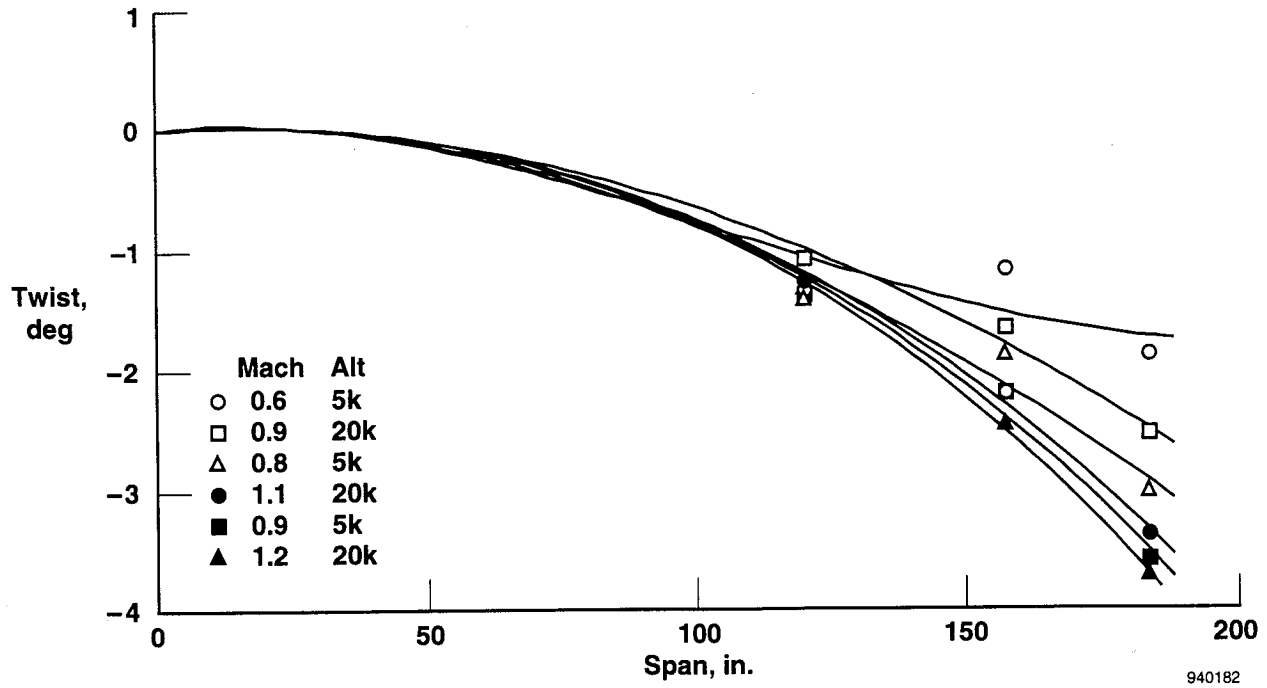

Fig. 9 Algorithm predicted twist vs span at 5*g*.

to become more negative with increasing Mach number. Second, twist is predicted to be less negative with increasing altitude. In all positive Nz maneuver cases the twist predicted is negative. This is commonly called wash-out, and is expected for typical aft swept wing configurations.

NASTRAN Predictions

While the NASTRAN model contained more than 32,000 grid points, certain grid points were identified which best represented key areas of the wing box structure. These grid points are shown in Figure 10. The areas of interest here are the front spar, rear spar, rib structures at wing span station, SS120, SS157, and the wingtip missile launch rail at SS185.25. The three span stations were selected to illustrate the chordwise behavior of the NASTRAN model under load. The elastic Z displacements of the grid points located along these three stations are shown in Figure 11. The load case applied here represents a 0.9 *M*, 5,000-ft altitude, 5-*g* pull-up with an advanced medium range air-to-air missile (AMRAAM) at each wingtip and a total aircraft gross weight of 24600 lb. As each span station is shown to deflect as a straight line, no chordwise bending prediction is indicated. Spanwise bending of the front and rear spars for 1 *g* and 5 *g* is shown in Figure 12. The difference in deflection between the front and rear spars is the basis for calculating the wing box twist which is shown in Figure 13.

Flight Data

The flight maneuvers were flown in sets of three; a 1-*g* cruise interval, a 3-*g* pull-up, and a 5-*g* pull-up. Each set required approximately one minute of flight time. Of the many available maneuver data sets, 11 were selected which would provide an adequate matrix for investigating the effects of Mach, altitude, external wing stores, and gross weight on wing twist under maneuver load. In each case the 5-*g* pull-up

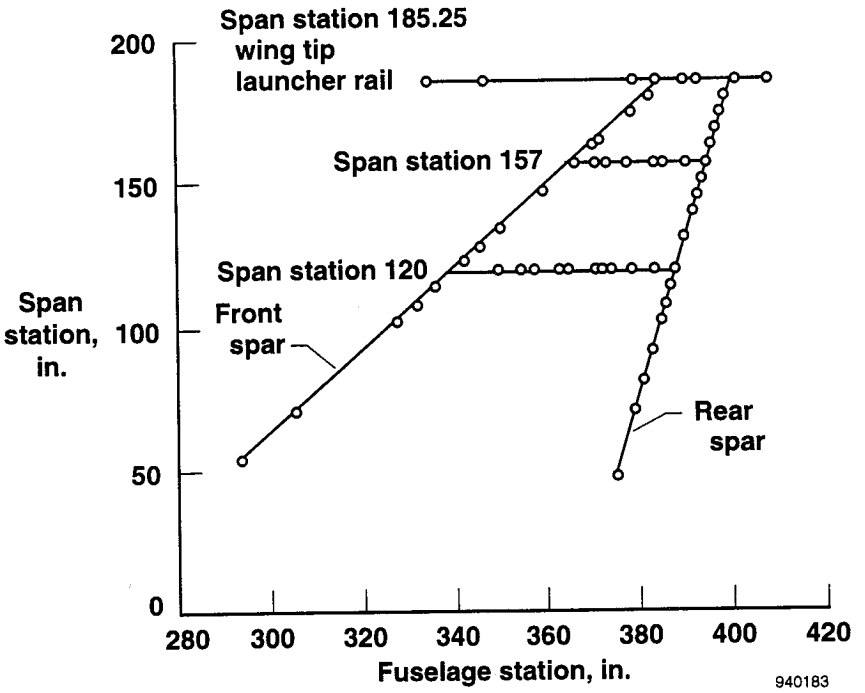

Fig. 10 Selected NASTRAN grid points.

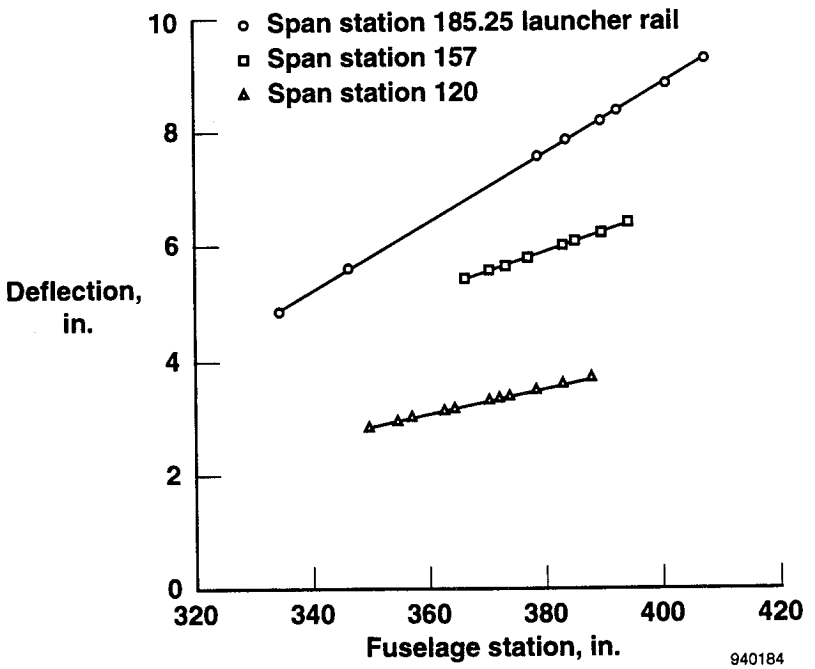

Fig. 11 NASTRAN displacements at three span stations vs fuselage station at 5*g* for a typical pull-up.

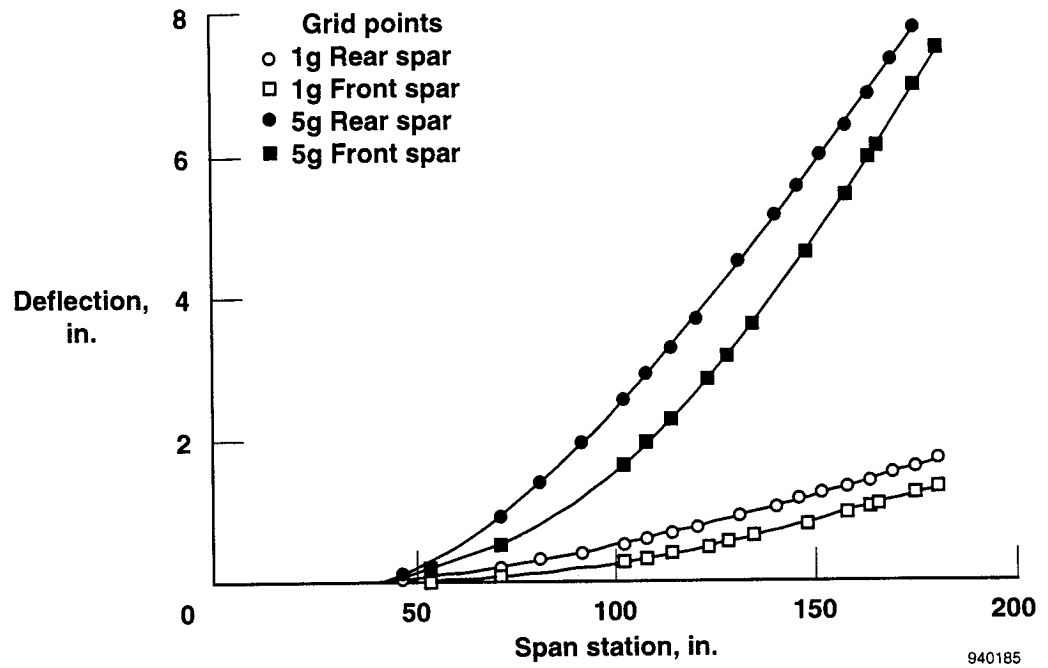

Fig. 12 NASTRAN front and rear spar deflections vs span station for a typical pull-up.

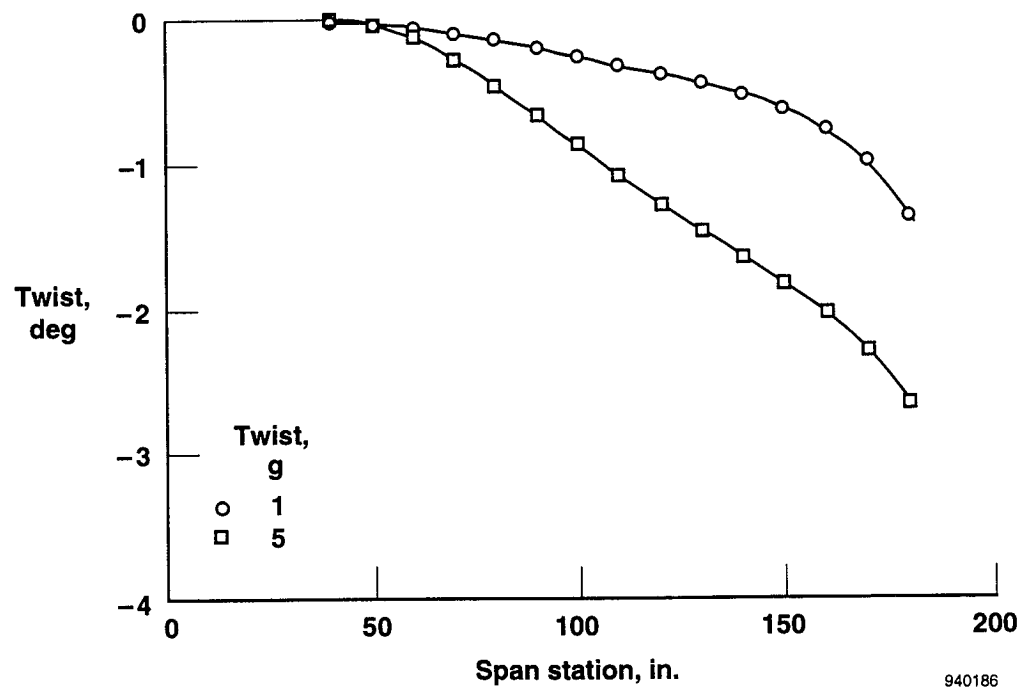

Fig. 13 NASTRAN wing box twist vs span for a typical pull-up.

was studied as it provided the widest range of elastic wing deformation. Figure 14 shows a normal acceleration time history for a typical 5-*g* pull-up maneuver. The indicated interval was selected for study since experience with similar data from the X-29A flight research program[3] has shown that the most smoothly increasing Nz part of a maneuver gives the cleanest and most repeatable deflection data with the least scatter and hysteresis. The elastic deflection of the aft tip target is plotted versus Nz in Figure 15, illustrating the curve fitting approach that was used to characterize the flight-measured deflection data. A standard polynomial curve fitting routine was used. The resultant calculated twist error band is minimized through the use of this curve fitting approach. Using the equation of the deflection versus Nz curve for each target, the deflection of each target was calculated for 5*g*s. These deflections plotted versus fuselage station are shown in Figure 16. Shown in this form these data reveal some mild chordwise bending that was not predicted by NASTRAN. For example, the center target at SS170.17 is deflected approximately 0.36 in. out of line with the front and rear targets at that station. This is much greater than even the basic worst-case deflection resolution of ±0.044 in. for that station (Fig. 7) and so is not the result of measurement error. In addition to some slight chordwise wing bending, some bending of the wingtip launcher rail is also evident. When the calculated 5-*g* deflections of the front and rear spar targets are plotted versus span station, as they are in Figure 17(a), the differential displacement of the front spar relative to the rear spar can be seen. This is the basis of the elastic streamwise twist calculation, which is shown in Figure 17(b). Because of the launcher rail flexibility, the wing box twist for the tip station is calculated from the differential displacement of the front and rear spars, and not the forward and aft launcher rail targets, to preclude that possible source of error.

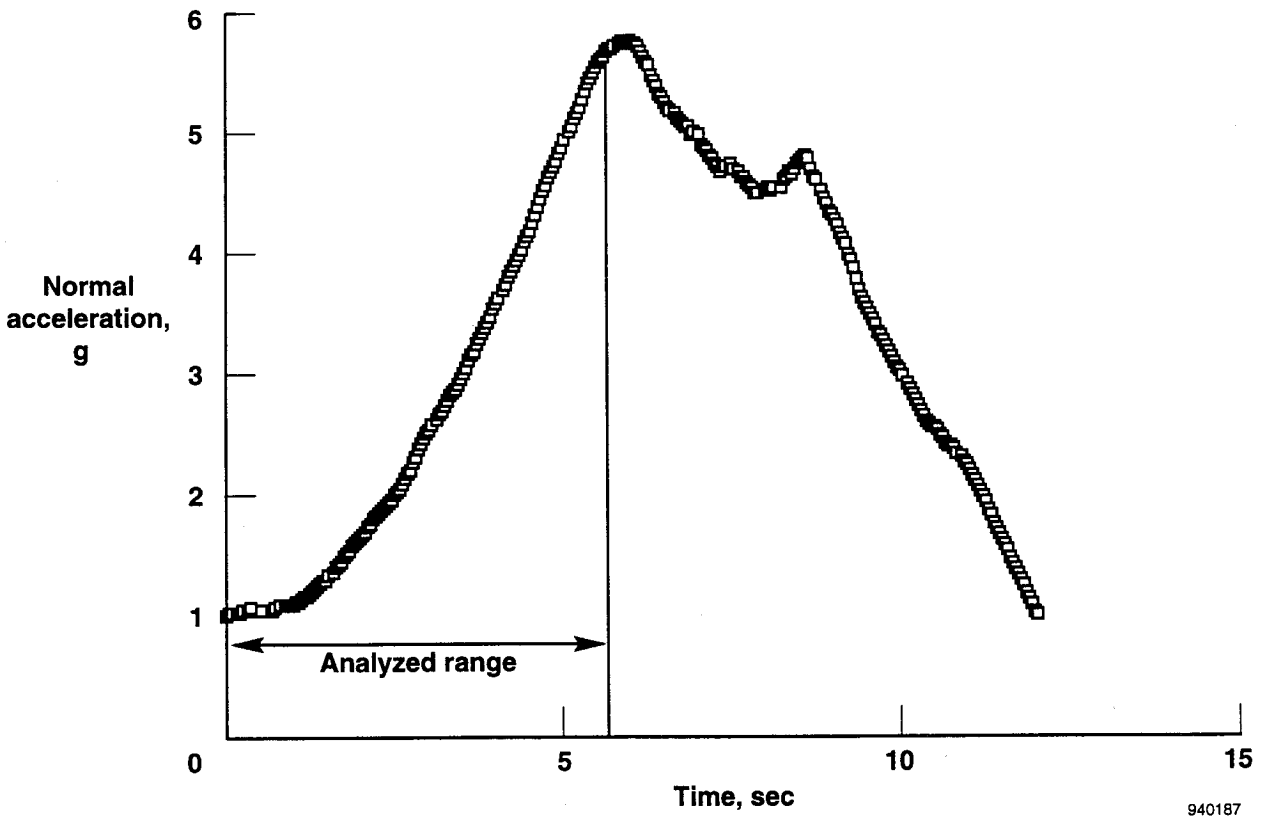

Fig. 14 Normal acceleration time history for a typical 5-*g* pull-up.

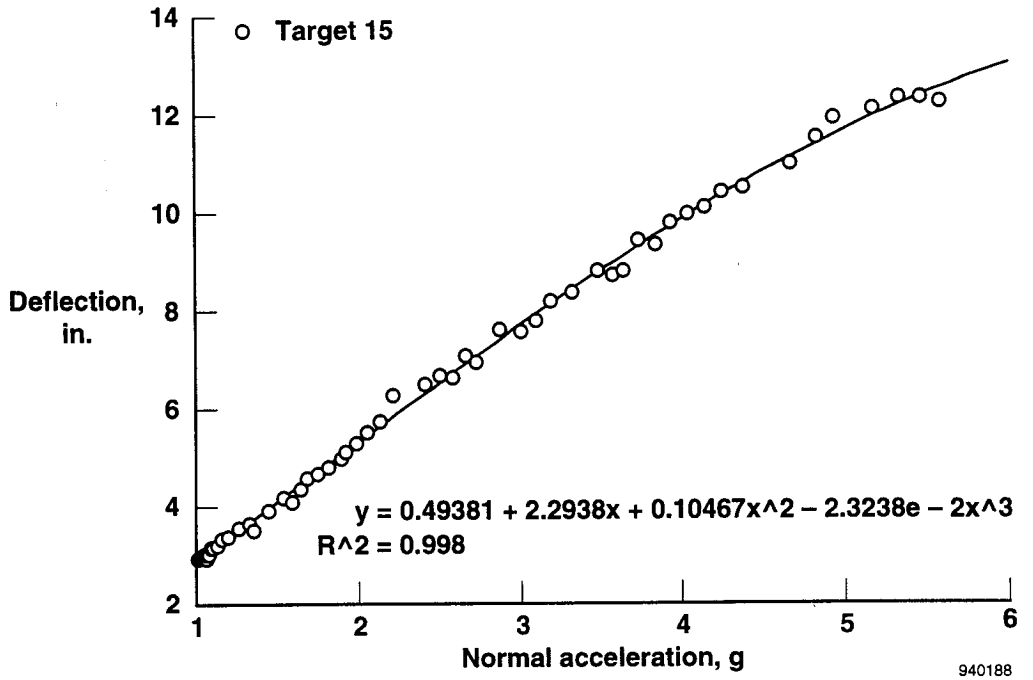

Fig. 15 FDMS target displacement vs normal acceleration curve fitting for a typical 5-*g* pull-up.

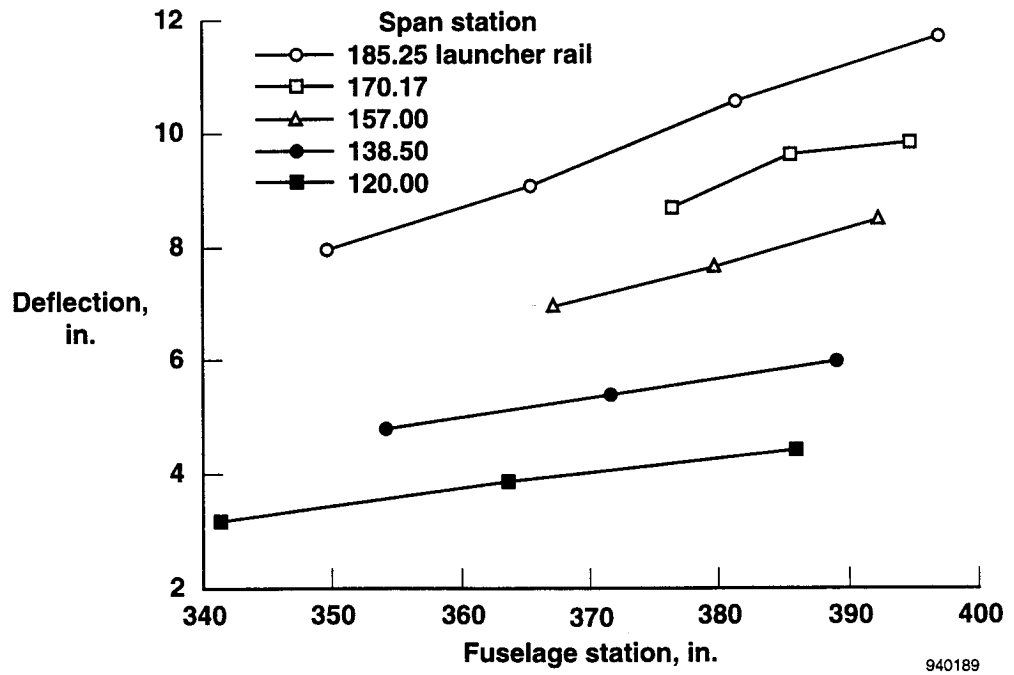

Fig. 16 FDMS displacements vs fuselage station showing chordwise bending at 5*g* for a typical pull-up.

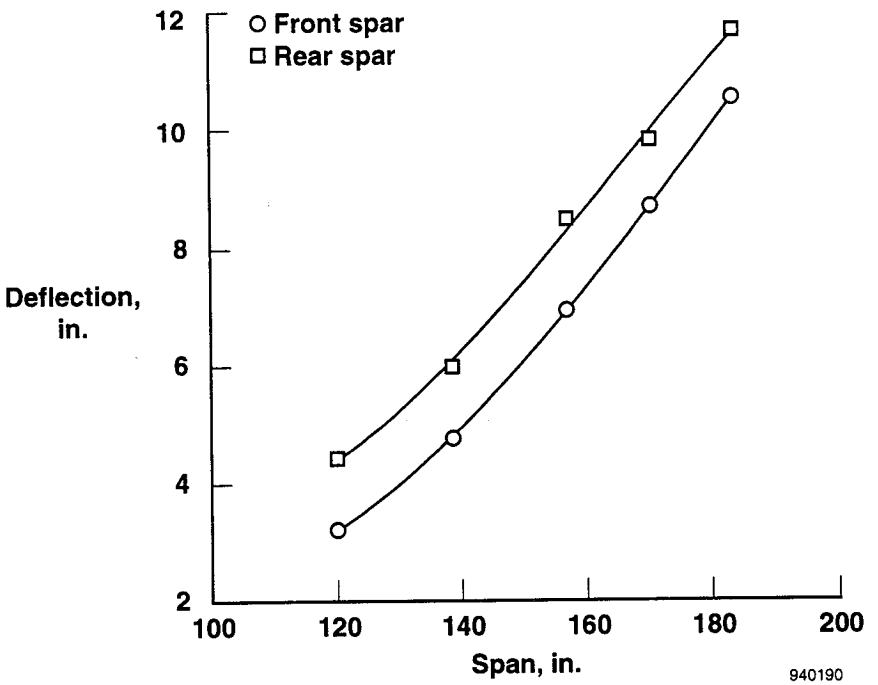

(a) Front and rear spar deflections.

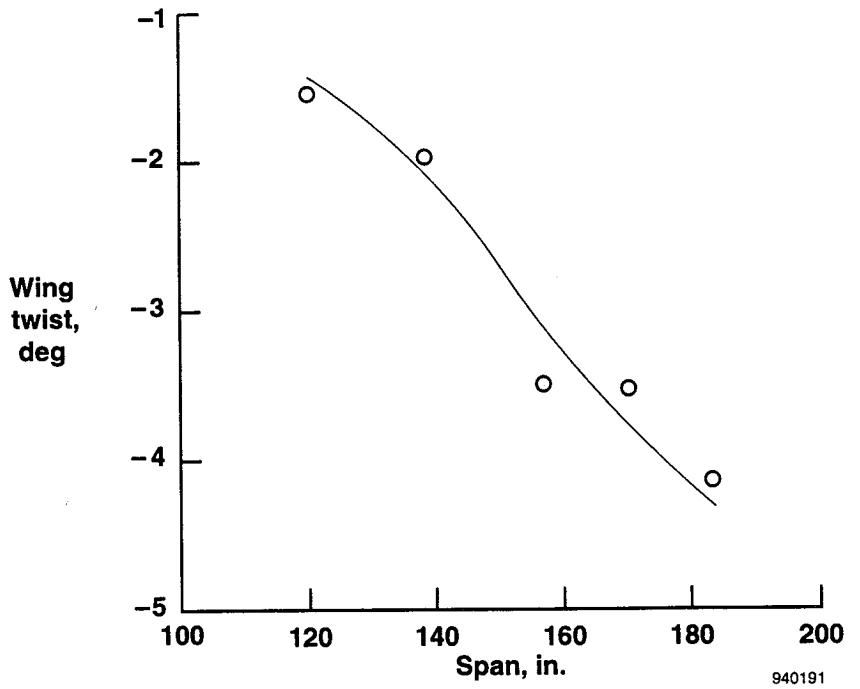

(b) Wing box twist.

Fig. 17 FDMS deflections and twists at 5*g* for a typical pull-up.

Parametric Analysis

In this section the effects of variation of Mach, altitude, underwing stores, and aircraft gross weight on wing box elastic streamwise twist will be examined using data from algorithm predictions, NASTRAN predictions, and flight measurements. The fuselage points of reference of these three sources of data are not coincident. The algorithm predictions are referenced to the aircraft INU, the NASTRAN model is constrained about the aircraft center of gravity (CG), and the FDMS reference is the receiver package. These references are different to the extent that the fuselage bends under load. The NASTRAN-predicted fuselage deflections for a 5-*g* maneuver loading were studied and it was determined that an offset of approximately 1/4° existed between the extremes of these references; the FDMS receiver package and the INU. This small offset has not been compensated for in the data comparisons that follow, however, this is transparent to the elastic twist increments that will be the focus of these comparisons.

Mach Effects

Figure 18 shows a comparison of 20,000-ft altitude, 5-*g* NASTRAN predictions, algorithm predictions, and flight-measured data at 0.9 *M* and 1.2 *M*. Although the gross weights and store loadings vary slightly between sources of data, the elastic wing twist increments due to Mach variation can be compared. The NASTRAN data indicated the smallest effect across the span, with the wingtip twist becoming 0.92° more negative for the increase in Mach number from 0.9 to 1.2. Inboard, this effect was much less noticeable. The flight-measured data showed the second largest effect across the span, but with only 0.15° more negative wingtip twist due to the increase in Mach number. Inboard, however, the difference was more significant. The largest increment was indicated by the algorithm-predicted curves, with 1.17° more negative twist at the wingtip due to the increase in Mach number. The algorithm overpredicted the elastic twist increment due to Mach number variation throughout the outer wing area.

Altitude Effects

Figure 19 shows a comparison of 0.9 *M*, 5-*g* NASTRAN and algorithm predictions, and flight-measured data at 5,000 and 20,000-ft altitude. The flight-measured twist curves show no change despite the change in altitude. These two maneuvers were flown back-to-back with the same stores load and nearly the same gross weight. The small gross weight change is caused only by the fuel burned from one maneuver to the next. The two NASTRAN-predicted curves likewise are for load cases that vary only by altitude and indicate a noticeable negative twist increment, measuring 0.75° at the wingtip, for the increase in altitude. The two algorithm-predicted curves are independent of gross weight and store loading and indicate a noticeable positive twist increment (opposite the NASTRAN indication) measuring 1.06° at the wingtip, for the increase in altitude. The algorithm overpredicted the elastic increment caused by altitude variation across the entire span. Although not the focus of this paper, the NASTRAN data were also in error. This could be due to inaccuracy in the NASTRAN structural model itself, or the predicted load sets applied to it.

Stores Effects

An aircraft's elastic wing twist is driven by net structural wing load and wing structural stiffness. The net structural wing loads are caused primarily by aerodynamic and inertial forces. Inertial forces are caused by mass being accelerated. In the case of a fighter aircraft wing, the effective wing mass is not only the wing structural mass but also includes the mass of any attached wing stores. Wing fuel, if it were

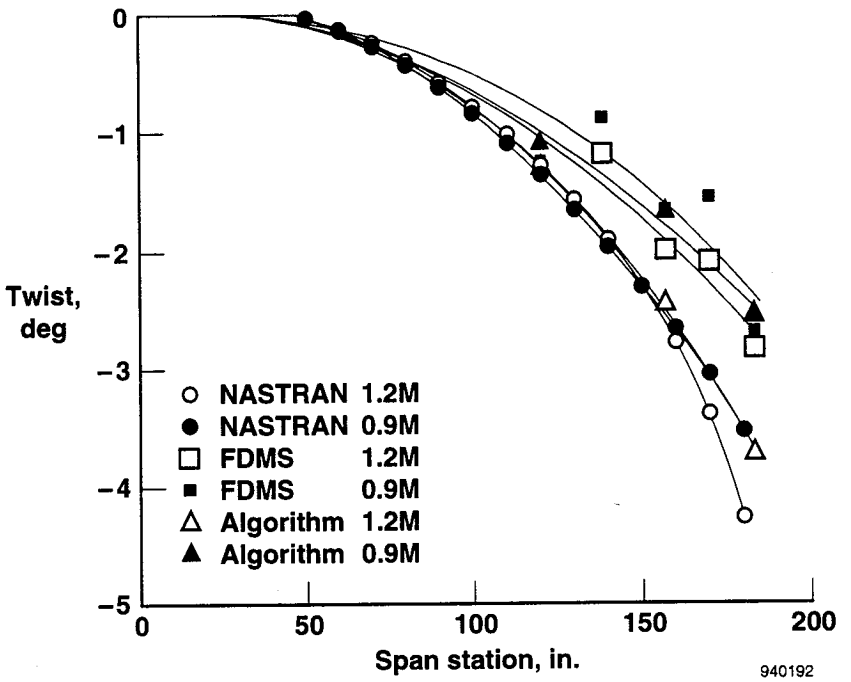

Fig. 18 Mach number variation effect, 20K, 5*g*.

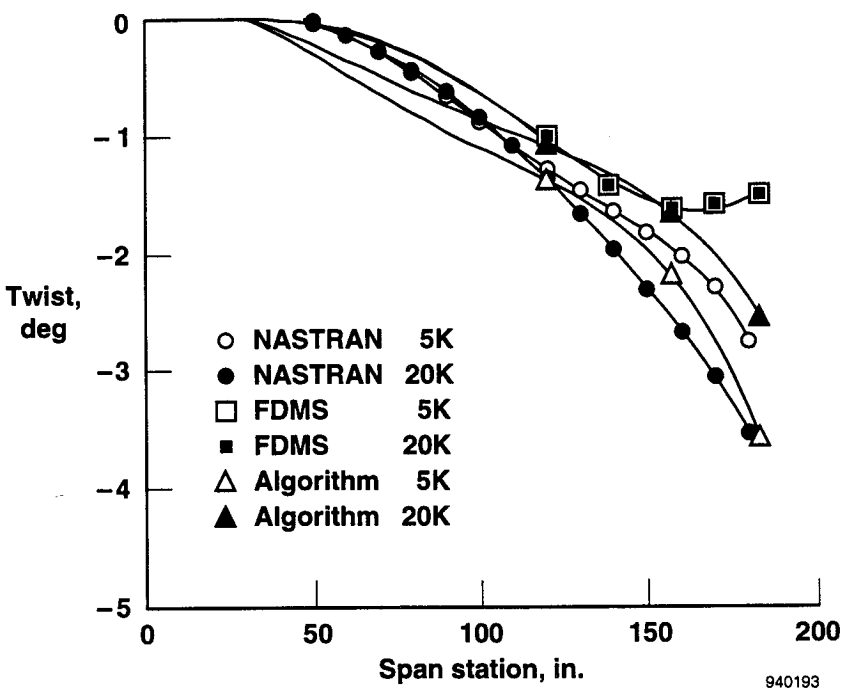

Fig. 19 Altitude variation effect, 0.9M, 5*g*.

present, would also contribute to this effective mass. Figure 20 illustrates the effect of wing external stores on wing box elastic twist under a 5-*g* maneuver load. NASTRAN-predicted curves are shown for three different wing store configurations. Two flight-measured twist curves are also shown. Starting with NASTRAN case 4, with one AMRAAM at each wingtip as a baseline, the effect of two store changes can be examined. NASTRAN predicts that with the addition of an MK84 2,000-lb iron bomb under each wing (at stations 3 and 7) that the twist becomes less negative. With the addition of two more AMRAAMs under each wing (at stations 2, 3, 7, and 8) instead of the MK84s, the twist becomes more negative. With the CG of these missiles forward of the wing's elastic axis, the inertial load of these stores adds torque to the existing wing aerodynamic torque load, producing more negative twist. The MK84s, with their CGs farther back, provide significant inertia relief with negligible, or opposite, torque addition, producing less negative twist. The flight data curves shown here illustrate only the effect of the addition of the MK84 under each wing. Here the resultant change in twist is in the same direction as indicated by the NASTRAN data, however it is much larger. The prediction algorithm does not take into account the aircraft's store configuration.

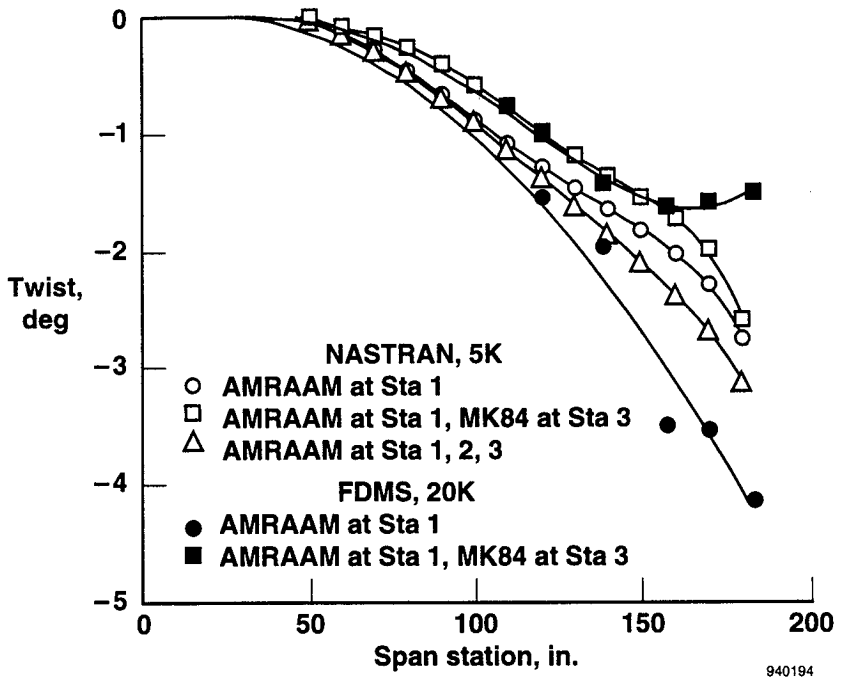

Fig. 20 Stores variation effect, 0.9M, 5*g*.

Aircraft Gross Weight Effects

For a given Nz, the wing loads can vary because of changes in aircraft gross weight, due to variations in remaining fuselage fuel (for example). This is why some aircraft flight load limits are regulated by a limit NzW value and not simply an Nz limit. Because wing loads change due to gross weight variation, so does the elastic wing twist. No pair of flight maneuvers was available in which only gross weight varied significantly. Figure 21 shows two NASTRAN-predicted elastic wing twist distributions. The only independent variable between the two curves is that the lower one represents a 23 percent higher gross weight than that of the top curve. It appears that the wingtip twist is dominated by the wingtip store (one AMRAAM) inertial load. Farther inboard however, NASTRAN predicts a noticeable difference between the

two. For example, at the 140-in. span station, the higher gross weight curve indicates 17 percent more negative twist. The prediction algorithm does not account for variations of aircraft gross weight.

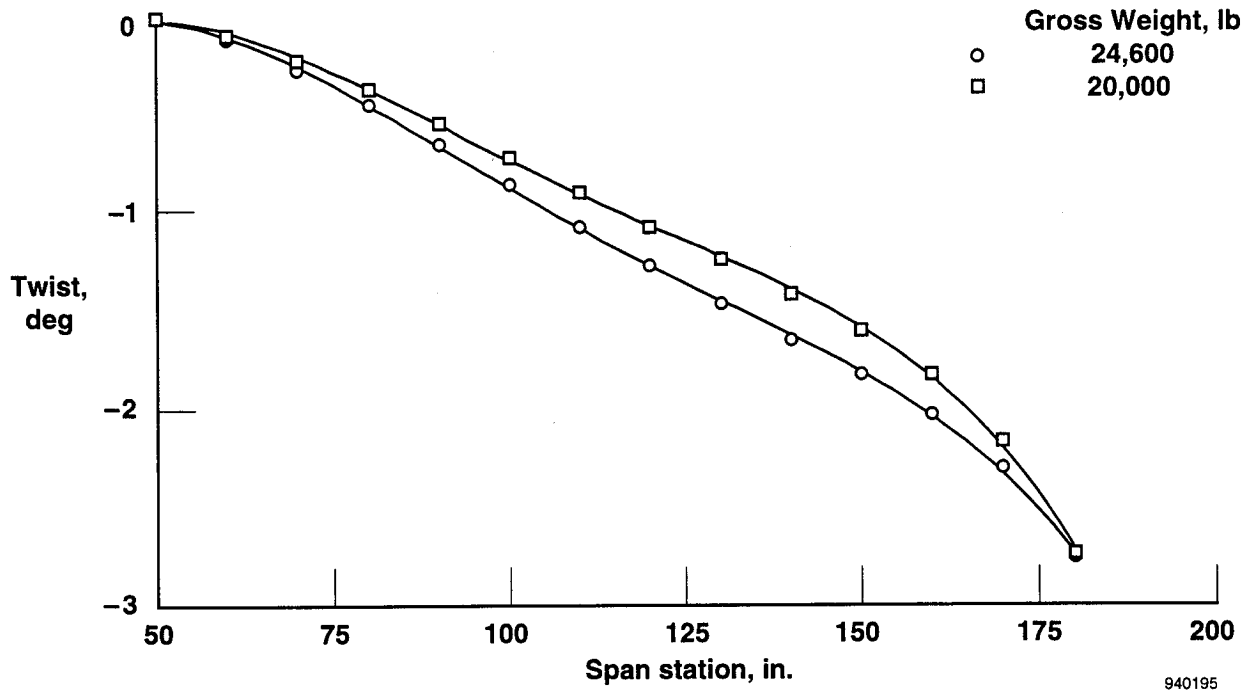

Fig. 21 NASTRAN gross weight variation effect, 0.9M, 5*g*, 5K, AMRAAM at stations 1 and 9.

CONCLUDING REMARKS

A study of the F-16C Block 40 aircraft's elastic streamwise wing box twist under flight load was performed using an existing real-time prediction algorithm, NASTRAN finite-element analysis, and electro-optical Flight Deflection Measurement System data to evaluate the existing prediction algorithm with new data to determine what improvements could be made. The existing algorithm predicts elastic twist at the different wing store stations as a function of aircraft Mach number, altitude, and normal acceleration. The FDMS and NASTRAN data indicated that refinements could be made to the existing algorithm by accounting for the effect of external wing stores, adjusting the coefficients for Mach number, accounting for variation of aircraft gross weight, and ignoring altitude. The new algorithm would then be a function of normal acceleration, stores configuration, Mach number, and gross weight. The coefficients for this new parameter list could be determined using the FDMS-produced database, as it was accurate and repeatable.

The authors thank Randolf C. Thompson, of PRC Inc., for providing expertise running NASTRAN on the CRAY computer.

REFERENCES

1. Jane's All the World's Aircraft 1989-90, John W.R. Taylor, ed., Jane's Information Group Limited (UK), 1989, pp. 412–415.

2. DeAngelis, V.M., "In-Flight Deflection Measurement of the HiMAT Aeroelastically Tailored Wing," AIAA-81-2450, Nov. 1981.

3. Lokos, William A., *Predicted and Measured In-Flight Wing Deformations of a Forward-Swept-Wing Aircraft*, NASA TM-4245, 1990.

4. Bonnema, Kenneth L., and William A. Lokos, "AFTI/F-111 Mission Adaptive Wing Flight Test Instrumentation Overview," ISA 35th International Instrumentation Symposium Proceedings, ISA Technical Paper 89-0084, May 1989.

5. DeAngelis, V. Michael, and Robert Fodale, "Electro-Optical Flight Deflection Measurement System," SFTE 18th Annual Symposium Proceedings, SFTE Technical Paper 22, Sept. 1987.

REPORT DOCUMENTATION PAGE

Form Approved
OMB No. 0704-0188

1. AGENCY USE ONLY (Leave blank)	2. REPORT DATE	3. REPORT TYPE AND DATES COVERED
	December 1994	Technical Memorandum

4. TITLE AND SUBTITLE

Determination of Stores Pointing Error Due to Wing Flexibility Under Flight Load

5. FUNDING NUMBERS

6. AUTHOR(S)

William A. Lokos, Catherine M. Bahm, Robert A. Heinle

7. PERFORMING ORGANIZATION NAME(S) AND ADDRESS(ES)

NASA Dryden Flight Research Center
P.O. Box 273
Edwards, California 93523-0273

8. PERFORMING ORGANIZATION REPORT NUMBER

H-2022

9. SPONSORING/MONOTORING AGENCY NAME(S) AND ADDRESS(ES)

National Aeronautics and Space Administration
Washington, DC 20546-0001

10. SPONSORING/MONITORING AGENCY REPORT NUMBER

NASA TM-4646

11. SUPPLEMENTARY NOTES

Presented as AIAA-94-2112 at the 7th Biennial Flight Test Conference, Colorado Springs, CO, June 20–23, 1994.

12a. DISTRIBUTION/AVAILABILITY STATEMENT

Unclassified—Unlimited
Subject Category 05

12b. DISTRIBUTION CODE

13. ABSTRACT (Maximum 200 words)

The in-flight elastic wing twist of a fighter-type aircraft was studied to provide for an improved on-board real-time computed prediction of pointing variations of three wing store stations. This is an important capability to correct sensor pod alignment variation or to establish initial conditions of iron bombs or smart weapons prior to release. The original algorithm was based upon coarse measurements. The electro-optical Flight Deflection Measurement System measured the deformed wing shape in flight under maneuver loads to provide a higher resolution database from which an improved twist prediction algorithm could be developed. The FDMS produced excellent repeatable data. In addition, a NASTRAN finite-element analysis was performed to provide additional elastic deformation data. The FDMS data combined with the NASTRAN analysis indicated that an improved prediction algorithm could be derived by using a different set of aircraft parameters, namely normal acceleration, stores configuration, Mach number, and gross weight.

14. SUBJECT TERMS

Elastic wing twist; F-16 wing deformations; In-flight deflection measurement; Wing store alignment

15. NUMBER OF PAGES

25

16. PRICE CODE

AO3

17. SECURITY CLASSIFICATION OF REPORT	18. SECURITY CLASSIFICATION OF THIS PAGE	19. SECURITY CLASSIFICATION OF ABSTRACT	20. LIMITATION OF ABSTRACT
Unclassified	Unclassified	Unclassified	Unlimited